Available online at www.sciencedirect.com
SCIENCE DIRECT®
PERGAMON
International Journal of Heat and Mass Transfer 46 (2003) 2799–2808
International Journal of HEAT and MASS TRANSFER
www.elsevier.com/locate/ijhmt

Radial mass-transfer enhancement in bubble-train flow ☆

Rainer Gruber, Thomas Melin *

Institut für Verfahrenstechnik der RWTH, Turmstr. 46, 52056 Aachen, Germany

Received 18 March 2002; received in revised form 9 January 2003

Abstract

Compared with single-phase laminar pipe flow, two-phase bubble-train flow shows a significantly increased rate of mass transfer between liquid and wall. The present work is a study of this effect over a wide range of the governing variables. The problem has been numerically simulated and experimentally examined using the copper dissolution method. Furthermore, a mathematical correlation for the Sherwood-number of the system is presented and the mechanism of transport enhancement is elucidated.

Keywords: Bubble-train flow; Two-phase flow; Capillary; Mass transfer; Enhancement

1. Introduction

This work is a study of mass transfer in a two-phase flow regime, known as bubble-train flow. This regime occurs when large gas bubbles are introduced into a liquid flowing laminarly through a duct with a small cross section. Under these circumstances, the bubbles or droplets adopt a characteristic capsular shape. They almost completely fill the cross section of the duct, remaining separated from the wall by a thin film of liquid.

Compared with single-phase laminar flow, bubble-train flow has two characteristics that are potentially useful: the axial segregation of the bulk liquid significantly reduces axial dispersion, while at the same time inducing a circulating flow pattern in the liquid, which enhances radial transport.

In the past, these effects have rarely been exploited. The primary technical application is in automated continuous-flow analysers, where bubble-train flow is used to separate samples from each other [1]. The effect of radial transport enhancement is a common observation in capillary blood vessels [2], but has not yet found its way into technical application beyond laboratory experiments. Given the recent interest in microprocess technology, this may change fundamentally in the near future: laminar liquid flow through micro-channels is characteristic of microprocesses and many micro-unit operations may profit from bubble-train flow.

The systematic exploitation of radial transport enhancement by bubble-train flow requires a reliable correlation of the parameters involved to quantify its effect. Despite the considerable attention given to two-phase pipe flows, the available literature does not satisfy this demand. There are several reasons for this shortcoming. First of all, many authors studied two-phase flow in pipes with a diameter larger than the capillary limit [3–6]. It has only recently been established, however, that the flow patterns observed at such diameters differ significantly from bubble-train flow [7].

Secondly, the majority of available studies are devoted to heat transfer, where the range of Prandtl-numbers is smaller by several orders of magnitude than the corresponding Schmidt-numbers in mass transfer. The results from heat transfer studies can thus only be applied to mass transfer by a speculative extrapolation.

Thirdly, none of the previous studies have been broad enough to form the basis for a generalised correlation. This is hardly surprising, given the large number of free parameters involved, which results in an insurmountable task if the necessary data are to be collected by experiment.

☆ This work was supported by a grant from the Deutsche Forschungsgemeinschaft.
* Corresponding author.
E-mail address: melin@ivt.rwth-aachen.de (T. Melin).
URL: http://www.ivt.rwth-aachen.de.

0017-9310/03/$ - see front matter
doi:10.1016/S0017-9310(03)00053-X

Nomenclature

A_w	surface area of the inner wall of the capillary (m^2)
Bo	Bond-number, $Bo = \Delta\rho g d_i^2/\sigma$ (–)
C	molar concentration ($kmol\,m^{-3}$)
Ca	Capillary-number, $Ca = \eta u_B \sigma^{-1}$ (–)
D	Fickian diffusion coefficient ($m^2\,s^{-1}$)
d_i	tube diameter (m)
E	enhancement factor, $Sh_{\text{bubble-train}} Sh^{-1}_{\text{single phase}}$ (–)
$E_{(\beta)}$	distribution density function of bubble lengths (–)
g	gravitational acceleration, $g = 9.81$ ($m\,s^{-2}$)
Gz	Graetz-number, $d_i^2 \bar{u} D^{-1} l^{-1}$ (–)
k_L	mass transfer coefficient between liquid and wall ($m\,s^{-1}$)
l	axial length (m)
$\dot{n}''$	molar flux ($kmol\,m^{-2}\,s^{-1}$)
Pe	Peclet-number, $Pe = u d_i D^{-1}$ (–)
r	radial coordinate, $0 \leqslant r \leqslant R$ (m)
R	tube radius (m)
Re	Reynolds-number, $Re = d_i u \nu^{-1}$ (–)
Sh	Sherwood-number, $Sh = k_L d_i D^{-1}$ (–)
$\bar{u}$	volume-average liquid velocity ($m\,s^{-1}$)
$\dot{V}$	volume flow rate ($m^3\,s^{-1}$)

Greek symbols

β	dimensionless distance between bubbles, $\beta = l_{\text{plug}} d_i^{-1}$ (–)
γ	dimensionless axial coordinate, $\gamma = z/d_i$ (–)
δ	dimensionless thickness of film between bubble and wall, $h d_i^{-1}$ (–)
ϵ	void fraction, $\epsilon = \dot{V}_{\text{gas}}/\dot{V}_{\text{tot}}$ (–)
ζ	dimensionless bubble length, $\zeta = l_{\text{bubble}} di^{-1}$ (–)
ν	kinematic viscosity ($m^2\,s^{-1}$)
ρ	density ($kg\,m^{-3}$)
σ	surface tension ($N\,m^{-1}$)

General subscripts

bubble	in/of a gas bubble
gas	in/of the gas phase
liq	in/of the liquid phase
plug	in/of a liquid plug
w	wall
α	value at entrance to the capillary
ω	value at exit from capillary

It is therefore no coincidence that the only attempt at devising a general model took a purely theoretical approach: Duda and Vrentas [8,9] studied the flow pattern and heat transfer in bubble-train flow by solving the boundary value problem analytically. Besides the geometric simplifications they had to introduce to solve the partial differential equations, their work suffers the drawback that their analytical solution takes the form of a system of implicit infinite series. Evaluating the solution requires extensive numerical effort, making its use impractical.

To our knowledge, there is only a single experimental study to date that directly addresses radial mass transfer in bubble-train flow. It was conducted by Horvath et al. [10], who used a tubular reactor to measure mass transfer. Although limited in scope, the study supplies some valuable reference data and allows the general conclusion that the rate of radial mass transfer in bubble-train flow lies between the values for single-phase laminar and turbulent flow.

In summary, only very little data and no general correlation of radial mass transfer in bubble-train flow are available. The objective of the present work is to fill this gap with a comprehensive study of the problem and to develop a corresponding correlation. The constraints placed by limited experimental resources on the scope of previous studies will be overcome by making extensive use of a numerical simulation of the problem. Nevertheless, the study will be restricted to capillaries with a circular cross section, to Newtonian liquids and to a dilute solute, since a departure from these three constraints would require a fundamentally different approach. And finally, a constant concentration boundary condition alone will be considered, since the constant flux condition common in heat transfer problems is very rarely encountered in mass transfer.

2. Theory

2.1. Defining bubble-train flow

There is some confusion concerning the nomenclature for gas–liquid flow patterns in general and bubble-train flow in particular. The term "bubble-train flow" is used by Thulasidas et al. [11,12], while other authors refer to the same pattern as "slug-flow" [10,13], "plug-flow" [14] or simply as intermittent flow [15]. Since it is the most descriptive term, we shall use "bubble-train flow" to describe a radially symmetrical flow pattern characterised by a sequence of capsule-shaped bubbles which almost completely fill the cross section of the duct and are separated from the wall by a thin liquid film (Fig. 1).

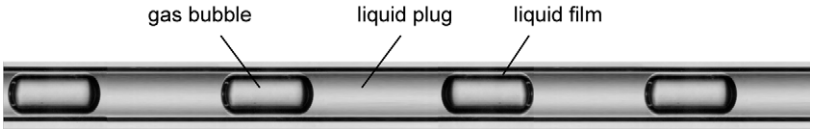

Fig. 1. Photography of bubble-train flow consisting of air bubbles in water flowing through a 1.2 mm glas capillary. The capillary is submersed in water to reduce refraction.

Radial symmetry is an important feature of bubble-train flow and in non-vertical flow it only occurs in tubes with a sufficiently small inner diameter to ensure a predominance of surface tension over buoyancy forces. The upper diameter limit of such tubes, which are referred to as capillaries, has been estimated by Suo and Griffith [13] on experimental evidence in terms of the Bond-number $Bo = \Delta\rho g d_i^2/\sigma$ as $Bo < 0.22$. For typical surface tension values, we find an upper diameter limit of between 1.5 mm (hydrocarbons) and 4 mm (pure water). Above this limit, stratification and bypass flows lead to a significant departure from the flow and transport regimes of bubble-train flow [7]. The present study is therefore limited to capillary tubes only.

2.2. Dimensional analysis

To reduce the number of free variables of the problem and enhance the generality of our findings, we shall express the quantitative analysis of mass transfer in bubble-train flow in terms of dimensionless groups. We have chosen the following seven groups:

$$Sh = \frac{k_L d_i}{D} \tag{1}$$

$$Re = \frac{d_i \overline{u}}{\nu} \tag{2}$$

$$Sc = \frac{\nu}{D} \tag{3}$$

$$\gamma = \frac{l_{\text{tube}}}{d_i} \tag{4}$$

$$\beta = \frac{l_{\text{plug}}}{d_i} \tag{5}$$

$$\zeta = \frac{l_{\text{bubble}}}{d_i} \tag{6}$$

$$\delta = \frac{d_{\text{film}}}{d_i} \tag{7}$$

Sh, Re, Sc and γ are the groups describing the classical Graetz–Nusselt problem of single-phase mass transfer in laminar pipe flow. To extend this set of groups to describe bubble-train flow, we merely need to include three dimensionless lengths describing the liquid plugs (β), the gas bubbles (ζ) and the thickness of the liquid film between bubble and wall (δ). In terms of these dimensionless groups, the objective of this work is to develop a correlation of the form

$$Sh = f(Re, Sc, \gamma, \beta, \delta, \zeta) \tag{8}$$

The choice of groups requires comment in several respects. First of all, we have decided to include the film thickness directly as a parameter instead of expressing it indirectly by a correlation of the Capillary-number Ca [16–18], since the principle tool of this study will be a numerical simulation in which the film thickness can be set explicitly. In doing so, we also tacitly assume a rigid bubble-shape independent of Ca, which seems justified by our observation that the moderate distortion of the rear meniscus of the bubble at higher flow velocities does not affect the rate of mass transfer between liquid and wall noticeably.

Secondly, the definition of the liquid mass transfer coefficient k_L in the Sherwood-number requires explanation. It is defined as the ratio of solute flux to driving concentration gradient

$$k_L = \frac{\dot{n}''}{\Delta C} \tag{9}$$

where the concentration gradient is customarily defined either as a local, an arithmetic mean or a logarithmic mean value. Since it follows naturally from a shell balance, we will use the log-mean gradient:

$$\Delta C = \frac{(C_{w,\alpha} - C_\alpha) - (C_{w,\omega} - C_\omega)}{\ln\left(\frac{C_{w,\alpha} - C_\alpha}{C_{w,\omega} - C_\omega}\right)} \tag{10}$$

Furthermore, the introduction of a second phase which is opaque to mass transfer introduces an ambiguity into the definition of $\dot{n}''$. It can either be defined as before as the flux per overall wall area

$$\dot{n}'' = \frac{\dot{V}_{\text{liq}}(C_\alpha - C_\omega)}{A_w} \tag{11}$$

or as the flux per surface area contacted by the plugs:

$$\dot{n}'' = \frac{\dot{V}_{\text{liq}}(C_\alpha - C_\omega)}{(1-\epsilon)A_w} = \frac{\dot{V}_{\text{tot}}(C_\alpha - C_\omega)}{A_w} \tag{12}$$

where $\epsilon = \dot{V}_{\text{gas}}/\dot{V}_{\text{tot}}$ is the void fraction of the flow. The rationale of this definition is that mass transfer from the film is negligible and thus only the surface between the liquid plugs and the wall actively participates in mass transfer.

Both definitions have their merit. By using Eq. (12), we obtain a Sherwood-number Sh_{plug} that describes the rate of mass transfer from an individual plug. As Horvath et al. [10] point out, Sh_{plug} thus conveys information about the relative magnitude of convective and diffusive transport in the liquid. On the other hand, using Eq. (11) results in a Sherwood-number Sh_{process} that represents the rate of mass transfer in the flow as whole and can be used directly in a global mass balance over the capillary.

Since in this study bubble-train flow is viewed as a means to enhance a mass transfer process, it would seem obvious to study the results in terms of Sh_{process}. We shall not do so, however, for the following reason: it will be shown that the bubble length does not affect the intensity of mass transfer from an individual plug. By analysing the results in terms of Sh_{plug} we can therefore neglect ζ which reduces the parameter domain by one dimension. Therefore the results of this study will be analysed in terms of Sh_{plug} using the following definition:

$$Sh_{\text{plug}} = \frac{k_{\text{L,lm}} d_i}{D} = \frac{\frac{\dot{V}_{\text{tot}} d_i (C_\alpha - C_\omega)}{A_{\text{w}} D}}{\frac{(C_{\text{w},\alpha} - C_\alpha) - (C_{\text{w},\omega} - C_\omega)}{\ln\left(\frac{C_{\text{w},\alpha} - C_\alpha}{C_{\text{w},\omega} - C_\omega}\right)}} \tag{13}$$

By introducing $C_{\text{w},\alpha} = C_{\text{w},\omega} = 0$ and

$$\frac{Gz_{\text{tot}}}{4} = \frac{\dot{V}_{\text{tot}} d_i}{A_{\text{w}} D} \tag{14}$$

where Gz_{tot} is the Graetz-number of the two-phase flow, we obtain:

$$Sh_{\text{plug}} = \frac{Gz_{\text{tot}}}{4} \ln\left(\frac{C_\alpha}{C_\omega}\right) \tag{15}$$

The analysis can later be extended to Sh_{process} by simple multiplication:

$$Sh_{\text{process}} = Sh_{\text{plug}}(1 - \epsilon) \tag{16}$$

Finally, it is also useful to express the enhancement of mass transfer in bubble-train flow in relation to single-phase mass transfer in terms of a process-enhancement factor E:

$$E_{\text{process}} = \frac{Sh_{\text{process}}}{Sh_{\text{single phase}}} \tag{17}$$

where both Sherwood-numbers refer to the same volumetric liquid flow rates. E is useful, since $E_{\text{process}} > 1$ is a straightforward criterion for process enhancement [1] by bubble-train flow.

[1] Enhancement implies either treating more liquid to the same specification or treating the same flow to a higher specification.

3. Experimental and computational study

The development of a correlation for the Sherwood-number of bubble-train flow involves two steps. First, a comprehensive data set comprising Sh over a wide range of parameters is created. Then, a mathematical expression for the correlation is developed and the free parameters of this model are determined by fitting the equation to the data set.

Classically, the first step is accomplished by a set of experiments. In the present case, however, the problem has six governing dimensionless variables, each with a wide range of values. Sampling this domain with a reasonable resolution would require an unfeasible experimental effort. Instead, the problem of data generation was tackled by numerical simulation, which lends itself very well to the kind of automated execution required here. In order to verify the simulations, a limited set of experiments were performed as well.

In spite of the principle suitability of commercial CFD-tools to generate a large data set describing the problem, it soon became clear that the greater efficiency of custom-written code was required to finish the task in reasonable time. To avoid reinventing the wheel in doing so, the following hybrid approach was developed. The commercial CFD-package Flow 3D (Flow Science, Los Alamos, USA) was used to solve the Navier–Stokes equations and determine the velocity field of the flow. Then a custom-written tool was developed to solve the conservation equation for the solute, based on the precomputed velocity data. The custom solver was written in Matlab (The Mathworks, Natick, MA, USA). In order to minimise the required number of Flow 3D jobs, the velocity data were cut into characteristic regions and reassembled with varying bubble and plug lengths. Thus, for every value of Re and δ, merely one Flow 3D simulation was required to calculate mass transfer at arbitrary values of β, γ, ζ and Sc.

For the experimental verification of the simulation, the copper dissolution method according to Gregory and Riddiford [19] was chosen. It involves contacting a copper surface with a solution of sulphuric acid and potassium dichromate. The dichromate anion acts as an oxidation agent and oxidises the copper according to the following over-all equation:

$$3\text{Cu} + \text{K}_2\text{Cr}_2\text{O}_7 + 7\text{H}_2\text{SO}_4 \rightarrow 3\text{CuSO}_4 + \text{K}_2\text{SO}_4 + \text{Cr}_2(\text{SO}_4)_3 + 7\text{H}_2\text{O} \tag{18}$$

where chromium is reduced from $\text{Cr}^{(\text{VI})}$ to $\text{Cr}^{(\text{III})}$. Gregory and Riddiford showed the reaction rate to be determined solely by the rate of mass transfer to the wall. Thus the log-mean mass transfer coefficient can be computed directly from the decline in $\text{Cr}^{(\text{VI})}$. The method was chosen because of the numerous references in the literature to its reliability and ease of use.

In single-phase trial runs, however, we observed a significantly higher rate of mass transfer than predicted by the well-known solutions to the Graetz–Nusselt problem. This error could be traced essentially to natural convection induced by the increased density of the copper-enriched solution near the wall. According to the original recipe [19], the fresh solution was 1 M in H_2SO_4 and 30 mM in $K_2Cr_2O_7$. By using a solution with the same acidity but 100-fold more dilute in dichromate, the error could largely be removed [20]. The cause for the remaining error could not be elucidated. However, an excellent fit was achieved after refitting the diffusion coefficient to the experimental data, resulting in $D = 1.3756 \times 10^{-9}$ m^2/s as opposed to $D = 0.907 \times 10^{-9}$ m^2/s reported by Gregory and Riddiford [19]. As Newman [21, p. 304] points out, the effective diffusivity observed in a chemically complex solution under one set of hydrodynamic and geometric conditions is not readily applicable to exactly the same solution under a different set of conditions. Gregory and Riddiford determined the diffusivity in a porous diaphragm cell [22], which differs in several respects from diffusion in laminar pipe flow. In this light, the shift in effective diffusivity appears plausible and we have based our analysis on the fitted diffusion coefficient.

3.1. Materials, equipment and procedure

All chemicals were Reagent Grade and were supplied by Merck KGaA, Germany. The solutions were prepared with deionised tap water. Copper capillaries with an i.d. of 1 mm and a length of 250 mm were bought locally. They were certified according to DIN 1787 SF-Cu to consist of 99.9% pure copper. In order to obtain a chemically uniform surface, the tubes were prepared for use by rinsing their lumen with a sequence of acetone, water, potassium dichromate solution (30 mM dichromate in 1 M sulphuric acid) and water. Each rinse lasted for 5 min during which a flow rate of approximately 40 ml/min was maintained. After the final rinse, the tubes were blown dry.

Several methods for creating a steady and defined flow of bubbles in the capillary were examined. Surprisingly, the methods described in the literature [7,10,11,23], which essentially involve passing gas and liquid through a T-connection, did not produce a bubble-train with constant and uniform plug and bubble lengths. This was probably caused by the smaller capillary diameter used in this study, which increases the erratic effects of surface tension on bubble formation.

Instead, a new method was developed that proved to be very reliable. A finely adjustable flow of feed solution was dispensed via a magnetic three-way valve from a thin PTFE nozzle (i.d. 0.25 mm) into a funnel. The liquid was drawn from the spout of the funnel and pumped through the copper capillary. The three-way valve periodically interrupted the flow to the funnel, causing air to be sucked into the capillary and leading to the formation of bubble-train flow. By precisely timing the opening and closing of the valve by means of an electronic switch, the lengths of both the bubbles and plugs could be adjusted very finely. The method proved very stable, displaying no measurable drift in bubble and plug sizes over time.

The following equipment was used (Fig. 2): The feed solution was pumped from a 2 l glass flask with the aid of a peristaltic pump (MCP peristaltic drive with a MS/CA 4-12 head with 12 rollers, Ismatec, Zürich, Switzerland). The magnetic valve was manufactured by Neuberger GmbH (Freiburg, Germany) and was made of EPDM. The funnel was custom-made of transparent PMMA, allowing the bubble formation to be observed. The bubble-train was pumped from the funnel with a second peristaltic pump, equipped with eight rollers (Reglo-Analog MS-2/8-160, Ismatec, Zürich, Switzerland). Since the peristaltic pump "chops-up" the bubble train flow, it was placed at the outlet of the capillary, thus operating in suction mode. The tubing used in the peristaltic pumps was supplied by the pump manufacturer and was made of either Tygon® or Viton®. The funnel was connected to the copper capillary by means of stainless steel tubing, while the exit of the capillary was connected to the pump with semitranslucent PTFE-tubing to allow observation. All connecting tubes had the same inner diameter as the copper capillary and were interconnected with PEEK couplings. The feed flask and the copper tube were placed in a thermostatic basin which was maintained at 25 °C.

The liquid flow rate was determined volumetrically. The length of the liquid plugs resulted from the ratio of the gas and liquid flow rates and was determined by photographing the flow in the PTFE tubing.

Blank test runs without a copper tube proved that there was no measurable sink for $Cr^{(VI)}$ in the system other than the copper. Furthermore, samples of

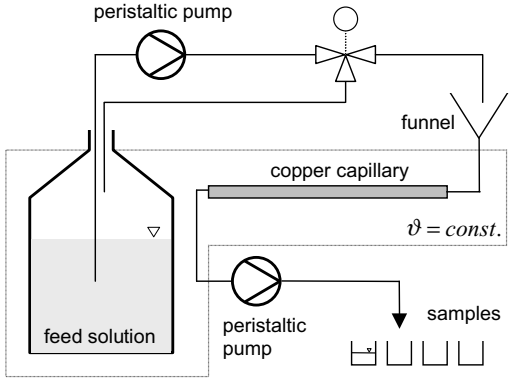

Fig. 2. Schematic representation of the experimental setup.

dichromate solution were left open to the air for 6 h without a measurable decline in $Cr^{(VI)}$ concentration, proving that no special precautions were required for sample handling.

Sampling began 10 minutes after starting the bubble-train flow through the capillary and three samples of 2.5 ml each were drawn at 2 min intervals for every run. Several runs were performed in one batch. The copper tubes were replaced after 8 h of operation and no significant change in inner diameter was detected.

The results were evaluated using a viscosity of $v = 1.01 \times 10^{-6}$ m^2/s [19] and the fitted diffusion coefficient of $D = 1.3756 \times 10^{-9}$ m^2/s.

4. Results

4.1. Experimental results and verification of numerical simulation

An early sensitivity analysis with the aid of the numerical simulation (see Section 4.2) showed that mass transfer is only weakly connected to the dimensionless bubble-length ζ and the dimensionless length of the capillary γ. By contrast, the dependence on Re and dimensionless plug length β is strong. We therefore decided to focus on these two variables in the experiments, which covered the range of Reynolds-numbers from $Re = 10$–50 and dimensionless plug lengths from $\beta = 10$–200. In the simulations, a film thickness of $\delta = 0.5\%$ was chosen as an estimate of the average experimental film thickness.

In Fig. 3, the experimentally observed relative exit concentrations are plotted over corresponding simulation results. The correlation between experiment and simulation is excellent. The standard deviation is $\sigma = 1.4\%$ and the errors are unsystematic.

By contrast, a comparison of the data reported by Horvath et al. [10] with simulations run with identical parameters is disappointing (Fig. 3). It shows a systematic deviation from the numerical results towards lower rates of mass transfer. In view of the excellent agreement between our experiments and simulations, we are inclined to seek the flaw in Horvath's data.

The potential source of error in the cited data arises from the enzyme-catalytic method used by the authors. They base their analysis on the crucial assumption that the reaction rate in their capillary reactor is entirely transport-limited. The evidence they cite is based on previous work [24] in which single-phase mass transfer was studied. Since, as will be shown, mass transfer in bubble-train flow is faster by up to an order of magnitude than its single-phase counterpart, this evidence of transport limitation may no longer be sufficient. If the enzyme-catalysed reaction at the wall introduces an additional resistance to turnover, this would be most

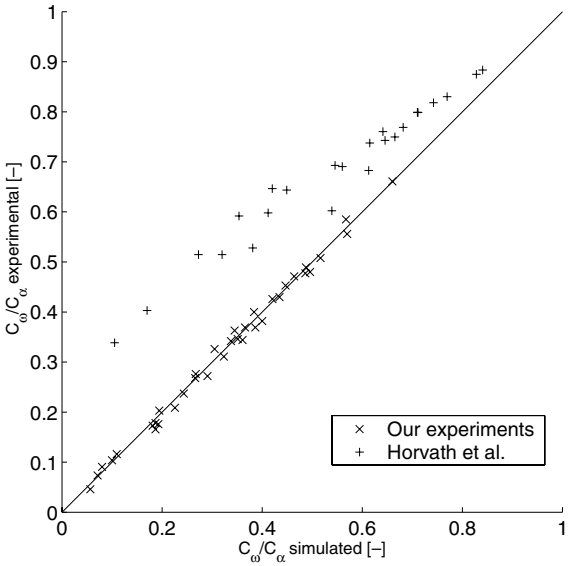

Fig. 3. Comparison of simulation and experiment. Our own experiments (×) coincide very well with the simulations. By contrast, data reported by Horvath et al. [10] (+) shows a lower rate of mass transfer than our results.

pronounced at the highest rates of mass transfer which occur in the shortest liquid plugs, which is supported by Fig. 3.

Although we could not resolve this issue finally, we consider the simulations verified on the evidence of their excellent agreement with our own experiments.

4.2. Sensitivity analysis

Before executing the main set of simulations, the sensitivity of mass transfer in bubble-train flow to the six governing free variables was examined by means of preliminary simulations. The purpose of this analysis was to focus the simulation work on the essential parameters and to identify regions of the parameter domain that require a higher resolution of samples.

The sensitivity study produced two essential findings. Firstly, the rate of mass transfer does not depend on Re and Sc independently but rather on the product of both, which is the Peclet-number $Pe = Re \cdot Sc$. This grouping is not surprising, since it is frequently observed in problems of heat and mass transfer. Secondly, Sh_{plug} proved insensitive to ζ and to δ up to $\delta \leqslant 0.01$. The latter holds easily for typical operating conditions, as has been shown in experimental and theoretical studies of the film thickness in bubble-train flow [16–18]. The problem was thus reduced to studying $Sh_{plug} = f(Pe, \beta, \gamma)$.

On the basis of the sensitivity study, the following domain for the remaining variables was chosen for the final simulations: $Pe = 1600$–$800\,000$, $\beta = 0.5$–600 with

higher resolution at the lower end of the scale and $\gamma = 0$–1000. In this way, some 15 000 data points were generated.

4.3. Presentation of results

The presentation of the four-dimensional data set obtained in the numerical simulation is not straightforward. The attempt to present the entire data set as a nomogram failed, since no suitable factorisation of Sh_{plug} could be found. Since the sensitivity study showed that Sh_{plug} reaches a steady value after entry effects have subsided, we have plotted Sh_{plug} over β and Pe at the limit of long capillaries (Fig. 4).

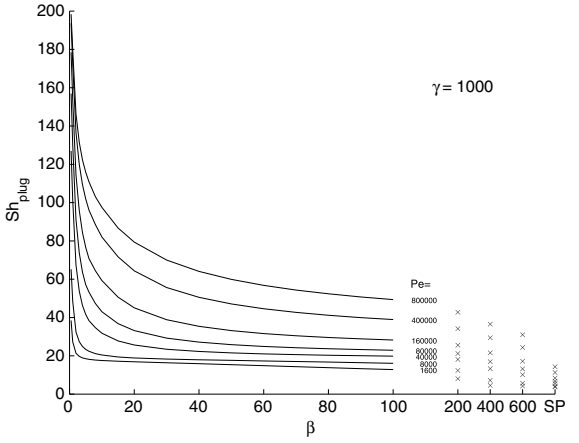

Fig. 4. Sh_{plug} for long capillaries ($\zeta = 1000$) over the dimensionless plug length β for several values of Pe. The single phase Sherwood-numbers are included for reference and are marked with SP. Data were generated by numerical simulation.

From an engineering point of view, bubble-train flow is a tool for process enhancement. The question thus arises, under which circumstances a process enhancement factor above unity is achieved. The analysis of the simulation results in terms of $E_{process}$ is difficult to present, since $E_{process} = f(Pe, Sc, \beta, \gamma, \zeta)$. Fig. 5, however, captures the characteristics of $E_{process}$ by plotting the data over the plug length for several bubble lengths at exemplary values of Pe and at a fixed capillary length of $\gamma = 200$.

The analysis of $E_{process}$ brought to light two remarkable findings. First of all, despite reducing the proportion of the wall actively participating in mass transfer by adding gas bubbles, it is virtually impossible to reduce process performance by bubble-train flow, unless very long bubbles with $\zeta > 100$ are permitted. Secondly, $E_{process}$ increases over the capillary length, since Sh_{plug} rapidly reaches a steady value while the single phase Sherwood-number continues to decrease to $Sh_s = 3.656$ [25, p. 165], which is the limit for a fully developed concentration profile. In other words, the longer the capillary, the more the process will be enhanced by bubble-train flow. And thirdly, while Sh_{plug} must clearly approach Sh_s at the limit of very long liquid plugs, we were surprised to find a significant effect of bubble-train flow even at $\beta = 600$, which were the longest plugs we simulated (Fig. 4). A linear extrapolation shows, that the effect of bubble-train flow on radial mass transfer only subsides at $\beta \approx 1100$.

4.4. The mechanism of flux enhancement

Besides the integral data for mass transfer presented in the previous section, the numerical simulation also enables us to elucidate the mechanism of flux enhancement

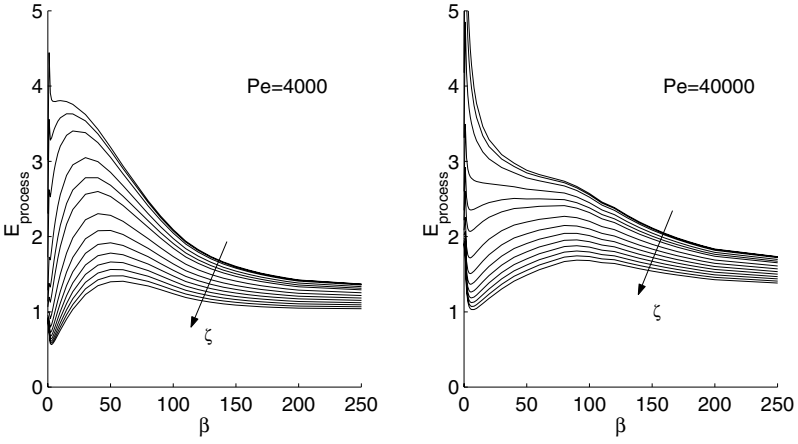

Fig. 5. The process enhancement factor $E_{process}$ plotted over plug lengths β for bubble lengths $\zeta \in \{2, 3, 5, 10, 15, 20, 30, \ldots, 100\}$. Data is plotted for $Pe = 4000$ (left) and $Pe = 40\,000$ (right).

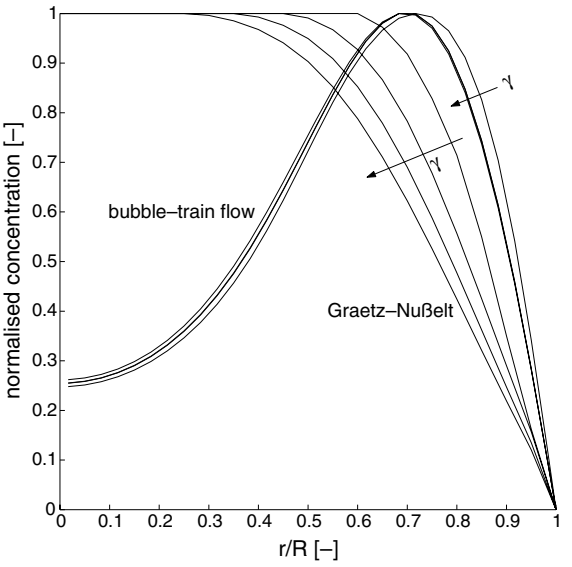

Fig. 6. Comparison of the radial concentration profiles in laminar single-phase and bubble-train flow. The profiles are plotted for $\gamma = 50$, 100, 150 and 200. The concentration profile in bubble-train flow was computed with $\beta = 20$ and was extracted from a position half-way between the bubbles. All concentrations were normalised.

by studying the evolving local concentration profiles during mass transfer.

In Fig. 6, the normalised radial concentration profiles in bubble-train flow and in the single-phase problem are compared. The single-phase profiles were calculated with the approximate solution to the Graetz–Nusselt problem presented by Skelland [25, p. 160 ff.], while the bubble-train concentration profile was taken from the numerical simulation at a position half-way between two bubbles. Both sets of data were sampled at $\gamma = 50$, 100, 150 and 200. [2]

The single-phase profiles show the expected gradual decay of the concentration gradient. By contrast, the normalised concentration gradient in bubble-train flow remains constant once it has been established and is steeper than its single-phase counterpart at the same axial position. It is this steeper concentration gradient near the wall that causes the enhancement to mass transfer observed in bubble-train flow.

4.5. Correlation

In devising a mathematical model, there is a choice between mechanistic and empirical modelling. Although there is merit in seeking to develop a mechanistic model, we found this route impractical, for several reasons. First of all, we were not able to cast the mechanism for enhanced mass transfer in bubble-train flow identified above into a handy mathematical framework. This failure is perhaps not surprising, since it has afflicted the exact solution of the Graetz–Nusselt problem as well, which takes the form of a multiple infinite series (see e.g., [25, p. 159 ff.]). All attempts at devising mathematically more wieldy solutions have either used simplifying assumptions that limit the validity of the solution (e.g., [26]) or have fitted purely empirical expressions to the exact solution (e.g., [27,28, p. 363]). Secondly and more critically, the issue of modelling the gradual exposure of the liquid plug to active wall area as it enters the capillary and in reverse as it exits from the capillary remains unresolved. For short plugs, this may not be critical, since the entry and exit take a short space of time and can thus be approximated as sudden complete entry and exit. This study has shown, however, that bubble-train flow enhances mass transfer appreciably even in very long plugs with dimensionless lengths in the order of $\beta > 1000$. For long plugs the entry and exit of the plug would make-up a sizable proportion of the overall process and cannot be approximated in this way. In view of these unresolved issues, it seems justified to abandon the mechanistic approach and take an empirical route to modelling.

The empirical model we have developed (Eq. (19)) is a product of three subfunctions. The first two functions represent the effects of Pe and β respectively and render Sh_{plug} at the limit of very long capillaries. The third function captures the entry effects which depend in sign and magnitude on both Pe and β and subside as a decay-function of γ. The model has 12 free parameters which were determined by fitting them to the results of the numerical simulation by a least-squares method. They are summarised in Table 1.

$$Sh_{\text{plug}} = a_1 \cdot \tanh(a_2 Pe^{a_3} + a_4) \cdot \tanh(a_5 \beta^{-a_6} + a_7) \cdot (1 - (a_8 Pe - a_9 \beta^{a_{10}} - a_{11}) \cdot e^{-a_{12}\gamma}) \quad (19)$$

The correlation has been fitted to data in the range of $Pe = 1.6 \times 10^3$ to 4×10^5, $\beta = 1$–600 and $\gamma = 30$–1000, but should be valid for larger values of β and γ as well. Within this range, it reproduces the results of the numerical simulation with an arithmetic mean error of

Table 1
Coefficients for use in Eq. (19)

$a_1 = 9.6699 \times 10^3$	$a_7 = 2.3378 \times 10^{-3}$
$a_2 = 6.1743 \times 10^{-4}$	$a_8 = 9.0380 \times 10^{-7}$
$a_3 = 5.9852 \times 10^{-1}$	$a_9 = 6.5869 \times 10^{-2}$
$a_4 = 1.1468 \times 10^{-1}$	$a_{10} = 4.6481 \times 10^{-1}$
$a_5 = 1.8897 \times 10^{-2}$	$a_{11} = 1.3620 \times 10^{-2}$
$a_6 = 4.6692 \times 10^{-1}$	$a_{12} = 2.8882 \times 10^{-2}$

[2] The data were computed using the exemplary values of $Re = 10$ and $Sc = 1000$; the findings hold for other levels of β, Re and Sc as well.

±10% and a maximum error of generally not more than ±20%.

Eq. (19) is applicable to a single liquid plug or a complete flow with uniform plug lengths. Under technical conditions, however, bubble-train flow will typically encompass a spread of plug and bubble sizes. It is therefore useful to extend Eq. (19) accordingly. Since the sensitivity analysis showed Sh_{plug} to be independent of the bubble length, the extension of Eq. (19) merely involves taking account of a spread of plug lengths.

Typically, a distribution of plug lengths is described by means of a distribution density function $E_{(\beta)}$, where $E_{(\beta)}\mathrm{d}\beta$ is the volume-fraction of all plugs flowing through the system that have dimensionless length between β and $\beta+\mathrm{d}\beta$. [3] Then the cup-mixing exit concentration is

$$\overline{C} = \int_0^\infty C_{(\beta)} E_{(\beta)}\,\mathrm{d}\beta \tag{20}$$

By introducing Eq. (20) into Eq. (13) we find the Sherwood-number for stochastic bubble-train flow:

$$\overline{Sh} = \frac{Gz_{\text{tot}}}{4}\ln\left(\frac{C_\alpha}{\overline{C_\omega}}\right) = \frac{Gz_{\text{tot}}}{4}\ln\left(\frac{C_\alpha}{\int_0^\infty C_{(\beta)}E_{(\beta)}\,\mathrm{d}\beta}\right) \tag{21}$$

We may express $C_{(\beta)}$ in terms of Sh_{plug} as defined by Eq. (19) by solving Eq. (13):

$$C_{(\beta)} = C_\alpha \exp\left(-\frac{4Sh_{(\beta)}}{Gz_{\text{tot}}}\right) \tag{22}$$

By inserting Eq. (22) into Eq. (21), we finally obtain the Sherwood-number for stochastic bubble-train flow, which can be evaluated numerically:

$$\overline{Sh} = -\frac{Gz_{\text{tot}}}{4}\ln\left(\int_0^\infty \exp\left(-\frac{4Sh_{\text{plug}}}{Gz_{\text{tot}}}\right)E_{(\beta)}\,\mathrm{d}\beta\right) \tag{23}$$

5. Conclusions

In this work, radial mass transfer in bubble-train flow through capillary tubes has been studied experimentally and numerically over a wide range of the governing variables, with two essential results.

First of all, the understanding of the bubble-train flow regime has been extended. The enhanced rate of mass transfer as compared to single phase laminar flow has been traced to the steeper concentration gradient at the capillary wall that is caused by the distinctive liquid flow pattern in bubble-train flow. The degree of enhancement has been found to depend strongly on the liquid Peclet-number and on the length of the liquid plugs, displaying the sharpest increase for very short plugs while remaining distinctly noticeable even for the longest plugs examined. In contrast to single-phase laminar flow, entry effects in bubble-train flow are brief and a steady Sherwood-number is rapidly reached.

Secondly, a mathematical correlation has been developed that predicts the rate of radial mass transfer in terms of a plug-Sherwood-number with reasonable accuracy.

From an engineering point of view, bubble-train flow is an attractive means to enhance radial mass transfer in small ducts and it has been shown to enhance process performance under virtually all circumstances. As Horvath et al. [10] point out, "the introduction of gas bubbles into the liquid stream does not create technical difficulties which would not be well compensated by the significant increase in radial transport". From our own experience, we can confirm this view. We therefore hope that this work will contribute to making bubble-train flow a standard tool for mass transfer enhancement.

[3] The exact shape of the distribution density function depends the method of creating the two-phase flow. For example, it may adopt a Gauss-distribution, in which case $E_{(\beta)} = 1/(\sigma\sqrt{2\pi})\exp(-(\beta-\overline{\beta})^2/2\sigma^2)$, where σ^2 is the variance and $\overline{\beta}$ is the average dimensionless plug length.

References

[1] L.T. Skeggs Jr., An automatic method for colorimetric analysis, J. Clin. Pathol. 28 (1957) 311–322.

[2] J. Prothero, A.C. Burton, The physics of blood-flow in capillaries—i. The nature of the motion, Biophys. J. 1 (1961) 565–575.

[3] H.A. Johnson, A.H. Abou-Sabe, Heat transfer and pressure drop for turbulent flow of air–water mixtures in a horizontal pipe, Trans. Am. Soc. Mech. Eng. 74 (1952) 977–987.

[4] H.A. Johnson, Heat transfer and pressure drop for viscous-turbulent flow of oil–air mixtures in a horizontal pipe, Trans. Am. Soc. Mech. Eng. 77 (1955) 1257–1264.

[5] D.R. Oliver, S.J. Wright, Pressure drop and heat transfer in gas–liquid slug flow in horizontal tubes, Br. Chem. Eng. 9 (1964) 590–596.

[6] D.R. Oliver, A. Young-Hoon, Two-phase non-newtonian flow—ii. Heat transfer, Trans. Inst. Chem. Eng. 46 (1968) 116–122.

[7] K.A. Triplett, S.M. Ghiaasiaan, S.I. Abdel-Khalik, D.L. Sadowski, Gas–liquid two-phase flow in microchannels, part i: two-phase flow patterns, Int. J. Multiphase Flow 25 (1999) 377–394.

[8] J.L. Duda, J.S. Vrentas, Steady flow in the region of closed streamlines in a cylindrical cavity, J. Fluid Mech. 45 (1971) 247–260.

[9] J.L. Duda, J.S. Vrentas, Heat transfer in a cylindrical cavity, J. Fluid Mech. 45 (1971) 261–279.

[10] C. Horvath, B.A. Solomon, J.-M. Engasser, Measurement of radial transport in slug flow using enzyme tubes, Ind. Eng. Chem. Fundam. 12 (4) (1973) 431–439.

[11] T.C. Thulasidas, M.A. Abraham, R.L. Cerro, Bubble-train flow in capillaries of circular and square cross section, Chem. Eng. Sci. 50 (1995) 183–199.
[12] T.C. Thulasidas, M.A. Abraham, R.L. Cerro, Flow patterns in liquid slugs during bubble-train flow inside capillaries, Chem. Eng. Sci. 52 (1997) 2947–2962.
[13] M. Suo, P. Griffith, Two-phase flow in capillary tubes, J. Basic Eng. 86 (1964) 576–582.
[14] C.A. Damianides, J.W. Westwater, Two-phase flow patterns in a compact heat exchanger and in small tubes, in: Proceedings of Second UK National Conference on Heat Transfer, Mechanical Engineering Publications, London, 1988, pp. 1257–1268.
[15] T. Fukano, A. Kariyasaki, Characteristics of gas–liquid two-phase flow in a capillary tube, Nucl. Eng. Des. 141 (1993) 59–68.
[16] F. Fairbrother, A.E. Stubbs, Studies in electro-endosmosis—iv. The bubble tube method for measurement, J. Chem. Soc. 1 (1935) 527–529.
[17] R.N. Marchessault, S.G. Mason, Flow of entrapped bubbles through a capillary, Ind. Eng. Chem. 52 (1960) 79–84.
[18] F.P. Bretherton, The motion of long bubbles in tubes, J. Fluid Mech. 10 (1961) 166–188.
[19] D.P. Gregory, A.C. Riddiford, Dissolution of copper in sulphuric acid solutions, J. Electrochem. Soc. 107 (1960) 950.
[20] R.F. Gruber, T. Melin, Mixed convection in the copper dissolution technique of studying mass transfer, Int. J. Heat Mass Transfer, doi:10.1016/S0017-9310(03)00011-5.
[21] J.S. Newman, Electrochemical Systems, second ed., Prentice-Hall, Englewood Cliffs, NJ, 1991.
[22] D.P. Gregory, A.C. Riddiford, Transport to the surface of a rotating disc, J. Chem. Soc. (1956) 3756–3764.
[23] A.M. Barajas, R.L. Panton, The effect of contact angle on two-phase flow in capillary tubes, Int. J. Multiphase Flow 19 (1993) 337–346.
[24] C. Horvath, A. Sardi, B.A. Solomon, Enzyme reactor tubes, Physiol. Chem. Phys. 4 (2) (1972) 125–130.
[25] A.H.P. Skelland, Diffusional Mass Transfer, Wiley, New York, 1974.
[26] M.A. Lévêque, Les lois de transmission de la chaleur par convection, Ann. des. Mines. 12 (1928) 201–299.
[27] H. Hausen, Darstellung des in Wärmeübergangs Rohren durch verallgemeinerte Potenzbeziehungen, Zeitschrift des Vereins Deutscher Ingenieure, Beiheft Verfahrenstechnik 4 (1943) 91–98.
[28] H.D. Baehr, K. Stephan, Wärme und Stoffübergang, Springer, Berlin, 1998.